Indirect search for dark matter with micrOMEGAs_2.4

G. Bélanger[1], F. Boudjema[1], P. Brun[2], A. Pukhov[3], S. Rosier-Lees[4], P. Salati[1], A. Semenov[5].

1) LAPTH, Univ. de Savoie, CNRS, B.P.110, F-74941 Annecy-le-Vieux, France
2) CEA,Irfu, Service de Physique des Particules, Centre de Saclay, F-91191 Gif-sur-Yvette, France
3) Skobeltsyn Inst. of Nuclear Physics, Moscow State Univ., Moscow 119992, Russia
4) LAPP, Univ. de Savoie, CNRS, B.P.110, F-74941 Annecy-le-Vieux, France
3) Joint Institute of Nuclear research, JINR, 141980 Dubna, Russia

Abstract

We present a new module of `micrOMEGAs` devoted to the computation of indirect signals from dark matter annihilation in any new model with a stable weakly interacting particle. The code provides the mass spectrum, cross-sections, relic density and exotic fluxes of gamma rays, positrons and antiprotons. The propagation of charged particles in the Galactic halo is handled with a new module that allows to easily modify the propagation parameters.

1 Introduction

Cosmological observations show strong evidence that our Universe contains a large amount of dark matter (DM). New weakly interacting massive particles (WIMP), such as those present in extensions of the Standard Model, have roughly the correct annihilation properties to fit the high precision cosmological measurements. Several astroparticle experiments are actively searching directly or indirectly for this new particle. Indirect detection of dark matter particles involves observation of the products of the DM annihilation in the galactic center, galactic halos or the extra galactic region. The annihilation products include positrons, anti-protons, anti-deuterons, gamma-rays and neutrinos. Recently many new results from indirect DM searches have been released. Hints of excesses that might be due to annihilation of dark matter particles have been reported although an interpretation of the measurements in terms of either DM annihilation or some astrophysical source has not been confirmed. PAMELA shows an excess of positrons relative to electrons between 10 and 100GeV [1] in agreement with earlier indications by HEAT [2] and AMS01 [3]. On the other hand PAMELA sees no excess in the antiproton spectrum [4]. Both Fermi [5] and ATIC [6] report an excess in the total electron plus positron spectrum but at energies of several hundred GeV's, much above those of PAMELA. Furthermore the electron spectrum measured by HESS [7] at very high energies is consistent with both Fermi and ATIC. The cosmic gamma-rays from the galactic center or from galactic sources have been probed in a wide energy range by INTEGRAL [8], Veritas [9], EGRET [10], as well as HESS [11, 12] and Fermi [13]. These observations lead to upper bounds on the DM annihilation cross section that are however strongly dependent on the halo profile, the propagation parameters and the background that is assumed for the standard astrophysics processes. Observations in all channels are being pursued actively with in particular Fermi and HESS taking data as well as AMS02 to be launched in 2010.

The interpretation of the recent and upcoming data requires tools to compute accurately the signals of DM annihilation in various channels and this in the context of different particle physics models. The purpose of the package presented here is to compute indirect signals in γ, e^+ and $\bar{p}$ produced in DM annihilations in the Galaxy. This package is presented as a new module of `micrOMEGAs` [14, 15], a code that computes the dark matter relic density, the elastic scattering cross sections of WIMPs on nuclei relevant for direct detection as well as the cross sections and decay properties of new particles relevant for collider studies.[1] `micrOMEGAs` includes several models of particle physics that predict a new stable weakly interacting neutral particle, the minimal supersymmetric standard model(MSSM) and several of its extensions, models with extra dimensions or the little Higgs model as well as facilities to incorporate new models [16]. As in earlier versions, `micrOMEGAs` provides the cross sections for dark matter annihilation into SM particles and the spectrum for γ, e^+ and $\bar{p}$ at the source. The propagation of charged particles through the Galaxy which strongly distorts the charged particles spectra is the main addition in this version.

The main features included in the indirect detection module are:

- Annihilation cross sections for all 2-body tree-level processes for all models.

- Annihilation cross sections including radiative emission of a photon for all models.

- Annihilation cross sections into polarised gauge bosons.

- Annihilation cross sections for the loop induced processes $\gamma\gamma$ and γZ^0 in the MSSM.

- Modelling of the DM halo with a general parameterization and with the possibility of including DM clumps.

- Integrals along lines of sight for γ-ray signals.

- Computation of the propagation of charged particles through the Galaxy, including the possibility to modify the propagation parameters.

- Effect of solar modulation on the charged particle spectrum.

- Model independent predictions of the indirect detection signals.

The neutrino spectrum originating from dark matter annihilation is also computed, however the neutrino signal is usually dominated by neutrinos coming from DM capture in the Sun or the Earth. The inclusion of this signature is left for a further upgrade.

In this paper we first review the procedure to obtain the flux of photons or antiparticles. This includes the computation of DM annihilation into SM particles and a description of the dark matter halo models. The propagation of charged particles including the issue of solar modulation is described in Section 4. The functions available in `micrOMEGAs` are described in section 5 [2]. Sample results as well as comparisons with other codes are presented in Section 6.

---

[1] DarkSUSY is another public code that computes the indirect signatures of dark matter annihilation [17]. It is confined to the minimal supersymmetric model.

[2] `micrOMEGAs`2.4 contains all the routines available in previous versions although the the format used to call some routines has been changed. In particular global variables are used to specify the input parameters of various routines. All functions of `micrOMEGAs` are described in the manual, manual4.tex, to be found in the main directory.

2 Fluxes from DM annihilation

Should primordial self-annihilation take place in the early Universe, the same process would take place nowadays in the denser regions of the Galactic DM halo. DM annihilation in the Galactic halo produces pairs of Standard Model particles that hadronize and decay into stable particles These particles then evolve freely in the interstellar medium. The final states with γ, e^+ and $\bar{p}$ are particularly interesting as they are the subject of indirect searches. The production rate of particles from DM annihilation at location $\mathbf{x}$ reads

$$Q_a(\mathbf{x}, E) = \frac{1}{2}\langle \sigma v \rangle \left(\frac{\rho(\mathbf{x})}{m_\chi}\right)^2 f_a(E) \ , \tag{1}$$

where σv is the annihilation cross-section times the relative velocity of incoming DM particles which we evaluate in the limit $v = 0$ (this is a good aproximation since $v = 10^{-3}$). Note that $\langle \sigma v \rangle$ includes averaging over incoming particles/antiparticles. For a Dirac particel where $\sigma_{\chi\chi} = 0$, $\langle \sigma v \rangle = 1/2\sigma_{\chi\bar{\chi}}$. m_χ is the mass of the DM candidate, $\rho(\mathbf{x})$ is the DM density at the location $\mathbf{x}$ and $f_a(E) = dN_a/dE$ is the energy distribution of the particle a produced in one reaction. The predictions for the energy spectra can also depend on some non perturbative effects including QCD and imply the use of Monte Carlo simulations.

2.1 Annihilation cross-sections and energy spectra

The cross-sections for the different 2-body annihilation channels of WIMPs are calculated automatically in any model implemented in `micrOMEGAs` [16]. This is done through the interface with `CalcHEP` [18]. All cross-sections are computed for a relative velocity $v = 0$. There is an option in the code to define another value for v. The continuum spectrum for γ, e^+, $\bar{p}$, ν production is calculated as follows.

The self annihilation of DM particles can occur at tree-level through 16 possible final states involving only pairs of SM particles. This includes all flavour diagonal pairs of fermions as well as gauge bosons, $\chi\chi \rightarrow q\bar{q}, l^-l^+, \nu_l\bar{\nu}_l, W^+W^-, ZZ$. Other final states involving R-parity even particles are also included, in particular the Higgs. In the MSSM this corresponds to all the channels with SUSY Higgs particles, namely $Zh_i, h_ih_j, W^\pm H^\mp$ and H^+H^- where h_i stands for h, H, A. For the basic channels, $q\bar{q}, l^-l^+, W^+W^-, ZZ$, we provide tables for γ, e^+, $\bar{p}, \nu$ production as obtained with PYTHIA version 6.4 [19]. The database has been processed with 2×10^6 events at 18 fixed energies corresponding to $10 < m_\chi < 5000$ GeV. Note that neutrons and antineutrons do not decay in PYTHIA, basically a $\bar{n}$ is considered to be a $\bar{p}$ and the small amount of energy lost in the β decay of $\bar{n}$ is neglected. For channels containing two different particles, AB, we obtain the final spectrum by taking half the sum of the $A\bar{A}$ and $B\bar{B}$ spectra. For channels with Higgses, or other particles whose mass are a priori unknown, we recursively calculate all $1 \rightarrow 2$ decay channels until we obtain particles in the basic channels. If during these decays we get a pair of particles AB where A is one of the basic channel, we suppose that half of the spectrum is obtained from $A\bar{A}$ and continue to decay B.

The γ and e^+ spectra can be substantially modified. First, polarisation of the gauge bosons final state can distort the positron and photon spectrum. Second, higher-order processes can also significantly modify the particle spectra. For example, photon radiation can strongly enhance some channels, this is particularly important for annihilation of a

Majorana DM candidate into light fermions which suffers a s-wave suppression. The additional photon removes this suppression and the cross section increases by several orders of magnitude [20]. The implementation of these two effects in `micrOMEGAs` are discussed in the following subsections. Finally at the one loop level, other final states are possible, such as $\gamma\gamma$, γZ^0, gg and γh^0. Although supressed by a factor α^2, the processes with γ's are nevertheless interesting since they lead to a spectacular signal, a mono-energetic γ ray line. The one-loop processes $\chi\chi \rightarrow \gamma\gamma, \gamma Z^0$ have been computed automatically with **Sloops** for the MSSM [21, 22], and are incorporated in `micrOMEGAs`. Note that the Majorana nature of the neutralino forbids an annihilation into γh^0 at rest.

2.1.1 Vector boson polarisation

The primary particles produced in DM annihilation are by default assumed to be unpolarised. In general however these particles and in particular vector particles can be polarised. For example the annihilation of neutralinos in the MSSM produces only transverse W's and Z's while the polarisation of spinor particles can be neglected because of the CP invariance of the initial state. The spectra after decay and hadronisation of standard particles extracted from PYTHIA also assumes unpolorized particles.

To take into account the polarisation, we include an option for gauge bosons pair production. The first step is to determine the degree of polarisation of the vector bosons produced via dark matter anihilation in a given model. We only need to determine the polarisation of one of hte vector bosons as only the $V_T V_T$ or $V_L V_L$ combinations are possible. To do this automatically, we compute with `micrOMEGAs` the three-body process $\chi\chi \rightarrow W^- e^+ \nu_e$ keeping only the contribution from W pair production followed with the W^+ leptonic decay. We then check numerically the angular distribution of ν_e in the rest frame of the on-shell W^+ with respect to the direction of flight of the W pair. The angular distributions are expected to be $3/8(1 + \cos^2\theta)d\cos\theta$ for W_T and $3/4(1 - \cos^2\theta)d\cos\theta$ for W_L. With this method, we can reconstruct automatically the W^+ polarisation in a generic model.

We then need the spectra of the stable particles produced after decay and hadronization of a polarised gauge boson. For this, two methods have been used and compared showing perfect agreement. In the first method, we pass to PYTHIA events with four outgoing particles representing the decays $W^+ \rightarrow 2x$ and $W^- \rightarrow 2x$ where the decay products are distributed according to the formulas presented above. For this we used PYTHIA 6.4 and the Les Houches event interface [23]. Initial events were generated only for $M_\chi = M_W$. Results for heavy CDM where obtained by boosting. The same procedure is also used for neutral gauge bosons. In the second method, a reweighting technique is applied within PYTHIA 6.4, by measuring event by event the θ angular distribution of the primary W (or Z) decay fermions in the boson rest frame. Namely, for each primary fermion a weight is determined depending on the polarisation assumption. For longitudinal polarisation it is equal to $\frac{3}{4} \times (1 - \cos^2\theta)$ while it becomes $\frac{3}{8} \times (1 + \cos^2\theta)$ for transverse polarisation as explained previously. Then for each stable particle ($\gamma, e^+\bar{p}, \nu$), the weight of the W (or Z) decay fermion they originate from, is used to build the energy spectrum for each polarisation scenario. This is done for 18 different CDM masses. Extensive comparisons of spectrum distributions for direct or reweighted longitudinally polarized bosons have been made. They are in perfect agreement. We also checked that the average of the polarised spectra obtained with each method agreed with the unpolarised one.

Taking into account the polarisation of the W's (or Z's) leads to a harder spectrum for e^+ originating from transverse W's than if the W's were assumed unpolarised. The polarisation effect corresponds to at most a factor of 3/2 increase for the most energetic charged particles. This is because both transversely polarised W give a harder spectrum while the spectrum for longitudinally polarised W vanishes at high energy, see fig. 1 for the positron spectrum. Both the polarised and unpolarised spectra are available in the `basicSpectra` routine. To calculate the spectra of DM annilation taking into account the polarisation of vector bosons one has to set a switch in the `calcSpectrum` routine, see the routines description in Section 4.
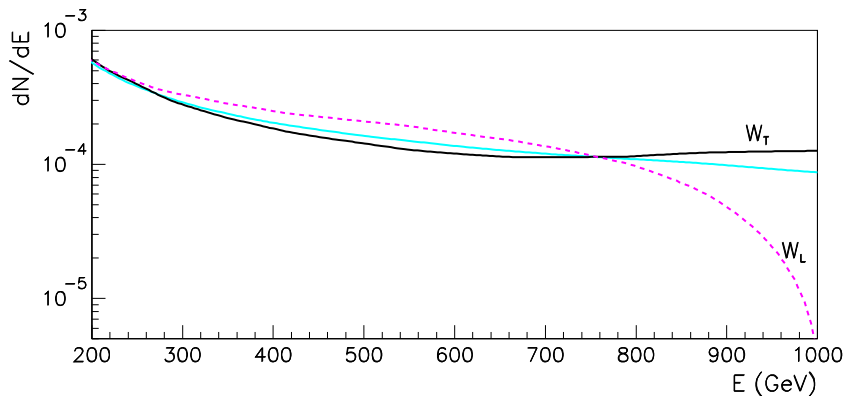

Figure 1: dN/dE for positrons from DM annihilating into W^+W^- with transversely polarised (full/black), longitudinally polarised (dash/pink) or unpolarised W's (full/blue), here $m_\chi = 1$ TeV.

2.1.2 Photon radiation

In a DM annihilation process, photons can be emitted from the external legs, final state radiation (FSR), from an internal leg, from a quartic vertex or in the subsequent decay of the pair of particles directly produced. The first two processes cannot be treated separately in a gauge invariant manner and are associated with a three-body annihilation process. They are a priori suppressed by a factor α, however large enhancements can occur [24]. In particular final state radiation features a collinear log corresponding to a photon emission from an external leg. This virtuality gives a factor $\log(4M_\chi^2/m_f^2)$ where m_f is the mass of the outgoing particle. For light particles final state radiation can therefore be approximated by the production cross section for two particles times a radiation factor that only depends on the spin of the particle. This is the approach followed in PYTHIA. Furthermore in the case of light masses $m_f \ll M_\chi$ one expects multiple photon radiation for the soft spectrum, this is also used in PYTHIA so that the FSR spectrum differs from the one corresponding to a single photon radiated from an external leg by up to 10% - 20% in the high energy part. For W bosons the virtuality is never large so photon radiation is ignored in PYTHIA, the only photons included in

PYTHIA are those coming from the decays of the gauge bosons. In this case a full $2 \rightarrow 3$ calculation is in order, however barring exceptional cases the yield is suppressed by a factor α (with no large logarithm enhancement) and therefore small. An important example where the approximation, and therefore applying PYTHIA, fails is if the cross section without radiation of a photon is for symmetry reasons very small or vanishing so that factorisation does not hold. A notable case, mentionned above, is the annihilation of the Majorana neutralino, at $v = 0$, to a pair of almost massless fermions. The s-wave cross section of order the chirality factor m_f^2/M_χ^2 can be much smaller than the radiation cross section of order α since the chirality argument no longer applies once a photon is radiated. The cross section including a photon emission can be enhanced in some specific cases. This can occur in situations where the t-channel particle exchanged between the DM particle and the external charged particle is not far from resonance, leading to an enhancement factor $M_\chi^2/(M_I^2 - M_\chi^2)$. M_I is the mass of the internal particle.

In our code we compute the direct photon production through the full $2 \rightarrow 3$ calculation, those are generated at run-time but only for the situation of interest which we have defined as $M_I^2 < 1.5 M_\chi^2$. We also compute the full $WW\gamma$ in situations where $M_\chi > 500$ GeV because of the potential large log enhancement due to photon emission since in this situation the W can be relativistic. All 3-body final states are included in the computation of the photon spectrum when this option is chosen. On the other hand only the $e^+ e^- \gamma$ process is included in the positron spectrum. Indeed these are the only processes that affect significantly the hard part of the positron spectrum.

When the full $\chi\bar{\chi} \rightarrow f\bar{f}\gamma$ process is generated by the code, one should avoid double counting due to the inclusion of the photons induced by PYTHIA through the direct $f\bar{f}\gamma$. By direct we mean the photons generated prior to the possible decays of f and hadronisation. To subtract the FSR contribution already taken into account in PYTHIA we remark that our generated $\chi\bar{\chi} \rightarrow f\bar{f}\gamma$ photon must exhibit the infrared divergent behaviour $1/x$, if the $\chi\bar{\chi} \rightarrow f\bar{f}$ cross section is not vanishing. This infrared behaviour at $x = 0$ can only originate from radiation from external charged legs. We therefore expand the generated $2 \rightarrow 3$ cross section of our code $d\sigma v/dx$ around $x = 0$ and write

$$\frac{d\sigma v}{dx} = \frac{A}{x} + B + Cx \tag{2}$$

The idea is to subtract from our generated cross section the A/x term for small enough x. For this we use $x = 0.01$. We have checked that $0.001 < x < 0.03$ give similar results. There might still be a mismatch between the coefficient A extracted from the full calculation and the one contained in PYTHIA. This difference is due to QCD hadronisation, higher order terms, additional photons and choice of the scale Q^2 for the splitting, contained in PYTHIA. To conform with the splitting function, for light fermions for example, we coud then subtract $A(1 - x + x^2/2)/x$, however in our code this hardly makes a difference in situations where the full calculation is important. At the level of implementation let us mention that there might be a problem caused by the finite precision of the phase space integration of the $2 \rightarrow 3$ matrix elements. For a fixed photon energy, there is an infrared pole when the outgoing fermion and the radiated photon become collinear. Furthermore strong numerical cancellations occur when summing over all diagrams. In the case of small fermion masses this can lead to numerical instability. To solve this we replace the integration variable $d\cos\phi$ to $d\phi$ (ϕ is the angle between the outgoing fermion and the radiated photon in the rest frame of the fermion pair). This trick works

well for $m_f < 10^{-4} m_\chi$. When $m_f < 10^{-3} m_\chi$ we keep $d\cos\phi$ as the integration variable and impose a cut $|\cos\phi| < 0.99$, in this region the numerical calculation is robust. The poles at $\phi = m_f/M_\chi$ due to radiation from the final charged particles are safely out of the integration region. We have tested that both methods are in good agreement when $m_f = 10^{-3} m_\chi$.

The importance of the extra contributions not contained in the factorised FSR to the photon spectra is illustrated in Fig. 2a for the CMSSM point $m_0 = 70$ GeV, $M_{\frac{1}{2}} = 250$ GeV, $A_0 = -300$ GeV, $\tan\beta = 10$. Here $M_\chi = 97.9$ GeV, $M_{\tilde\tau} = 107.6$ GeV, $M_{\tilde e} = M_{\tilde\mu} = 123.9$ GeV, neutralinos annihilate dominantly into tau pairs, this is an example of a case where the t-channel particle exchanged, the $\tilde\tau$, is not far from resonance so that photon radiation from internal lines is enhanced. Note that the curve denoted $\tau\tau\gamma$ in Fig. 2a represents only the contribution from the 3-body process, the additional photons that originate from τ decays are included when computing the full process. The enhancement in the high-energy part of the photon spectrum in a case where DM annihilation into gauge bosons pairs is dominant is illustrated in Fig. 2b for the MSSM. Here the DM is a mixed bino/higgsino LSP with $\mu = 545$GeV, $M_1 = 500$GeV, $M_3 = 6M_1 = 3M_2$, $\tan\beta = 20, M_A = 2$TeV and all soft sfermion masses heavy, $m_{\tilde f} = 2.5$TeV.
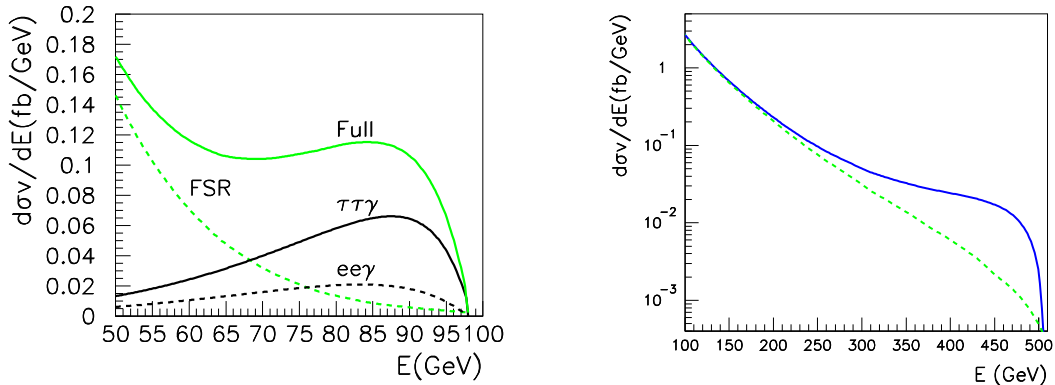

Figure 2: a) Photon spectrum for the CMSSM point $m_0 = 70$ GeV, $M_{\frac{1}{2}} = 250$ GeV, $A_0 = -300$ GeV, $\tan\beta = 10$ for $\chi\chi \to \tau^+\tau^-\gamma$ (black), $e^+e^-\gamma$ (black-dash), with photons from external legs from PYTHIA (FSR) (green-dash) and all contributions from 3-body final states (green-full). b) Photon spectrum for a MSSM point ($\mu = 545$GeV, $M_1 = 500$GeV, $\tan\beta = 20, M_A = 2$TeV and $m_{\tilde f} = 2.5$TeV) with (full) and without (dash) the contributions from the three-body process $\chi\chi \to W^+W^-\gamma$

2.2   Dark matter halo models

In `micrOMEGAs` routines which calculate the propagation of particles in the Galaxy the DM halo distribution is an input parameter. Thus `micrOMEGAs` can work with any spherically symmetric DM halo profile. As an example of DM halo distribution we include

a widely used spherically symmetric parametrization of the dark matter halo

$$\rho(r) = \rho_\odot F_{halo}(r)$$

$$F_{halo}(r) = \left[\frac{r_\odot}{r}\right]^\gamma \left[\frac{1 + (r_\odot/a)^\alpha}{1 + (r/a)^\alpha}\right]^{\frac{\beta-\gamma}{\alpha}} \tag{3}$$

The values for the α, β, γ and a parameters for the most common halo models are listed in Tab. 1, the default values are those of the NFW profile. The value of the DM density at the solar location $\rho_\odot$ and $r_\odot$ the distance of the Sun to the Galactic center are global parameters of `micrOMEGAs`. Their value can be redefined simply and the default values are listed in Table 3. An important remark concerns the central divergence. For $\gamma \geq 1.5$ in eq. 3 there is an non integrable squared density in the center of the galaxy. To avoid this singularity we set a limit for the distance from the Galactic center $r > r_{min} = 0.001pc$ in our integration routines. This is done for any halo profile.

Halo model	α	β	γ	a (kpc)
Isothermal with core	2	2	0	4
NFW	1	3	1	20
Moore	1.5	3	1.5	28

Table 1: Halo parameters for three common profiles

The user also has the possibility to use a totally different parameterization for the halo, provided it is spherically symmetric. For example the Einasto profile has been advocated recently [25]

$$F_{halo}(r) = \exp\left[\frac{-2}{\alpha}\left(\left(\frac{r}{r_\odot}\right)^\alpha - 1\right)\right] \tag{4}$$

where the default value for α is 0.17.

DM annihilation depends on the squared density $\overline{\rho^2}(r)$. In general a clumpy structure of DM will lead to $\overline{\rho^2}(r) > \overline{\rho}(r)^2$. The effect of clumping can be described by another profile

$$\overline{\rho^2}(r) = \rho_\odot^2 F_{halo}^2(r) F_{clump}(r) \tag{5}$$

The presence of clumps will lead to an enhancement factor or boost factor. In general the clump number density in a volume bounded by the characteristic diffusion length of the involved species will determine the size of the enhancement factor. The boost factor can therefore differ for photons, positrons or antiprotons. In the last two cases it does not typically exceed 20 [26] . Larger boost factors can be found for some extreme clump configurations, for example a big sub-halo close to the Earth [26], although this situation is very unlikely [27].

2.3   Photons

The gamma ray flux can be evaluated as

$$\Phi_\gamma(E, \phi) = \frac{\sigma v}{m_\chi^2} f_\gamma(E) H(\phi) \tag{6}$$

and is expressed in number of photons per $cm^2 s\ sr$. The factor H includes the integral of the squared of the dark matter density over the line of sight,

$$H(\phi) = \frac{1}{8\pi} \int_0^\infty dr \overline{\rho^2}(r')$$

(7)

where $r' = \sqrt{r^2 + r_\odot^2 - 2rr_\odot \cos\phi}$ and ϕ is the angle in the direction of observation. In `micrOMEGAs` one can compute the photon flux performing the integral over the line of sight and over the opening angle which characterizes the detector resolution, see section 4.

3 Galactic propagation of charged particles

3.1 General framework

The charged particles generated from DM annihilation propagate through the Galactic halo and their energy spectrum at the Earth differs from the one produced at the source. Charged particles are deflected by the irregularities of the galactic magnetic field. In the Milky Way which has strong magnetic turbulence Monte Carlo simulations indicate that this is described by space diffusion. Charged particles also suffer energy losses from synchroton radiation and inverse Compton scattering as well as diffusive reacceleration in the disk. Finally galactic convection wipes away charged particles from the disk. Solar modulation can also affect the low energy part of the spectrum. The equation that describes the evolution of the energy distribution for all particles (protons, anti-protons, positrons) reads

$$\frac{\partial}{\partial z} (V_C \psi_a) - \nabla \cdot (K(E) \nabla \psi_a) - \frac{\partial}{\partial E} (b(E) \psi_a) = Q_a(\mathbf{x}, E)$$

(8)

where $\psi_a = dn/dE$ is the number density of particles per unit volume and energy, a denotes the particle specie and Q_a is the source term. Here we do not consider background and include only particles produced from dark matter annihilation, Eq. 1. For antiprotons a negative contribution to the source term will also be considered to account for antiproton annihilations in the interstellar medium (see section 3.3). K is the space diffusion coefficient, assumed homogeneous.

$$K(E) = K_0 \beta(E) (\mathcal{R}/1 \text{ GV})^\delta$$

(9)

where β is the particle velocity and $\mathcal{R} = p/q$ its rigidity. $b(E)$ is the energy loss rate. Another term that describes the diffusive reacceleration has been neglected. The simple power law for $K(E)$ is inferred from magnetohydrodynamics considerations [29], once the convective velocity is taken into account it has been shown that this form for $K(E)$ was adequate to fit the B/C data [30].

The propagation equation, Eq. 8, is solved within a semi-analytical two-zone model which was discussed in [28, 30, 32]. Within this approach the region of diffusion of cosmic rays is represented by a thick disk of thickness $2L$ and radius $R \approx 20$ kpc. The thin galactic disk lies in the middle and has a thickness $2h \approx 200$ pc and radius R. The boundary conditions are such that the number density vanishes at $z = \pm L$ and at $r = R$. The galactic wind is directed outward along the z direction so the convective

9

velocity is also vertical and of constant magnitude $V_C(z) = V_C sign(z)$. The propagation parameters δ, K_0, L, V_C are constrained by the analysis of the boron to carbon ratio, a quantity sensitive to cosmic ray transport [30]. Typical values for these coefficients are listed in Table 2, default values are those of the MED model.

Model	δ	K_0 (kpc^2/Myr)	L (kpc)	V_C(km/s)
MIN	0.85	0.0016	1	13.5
MED	0.7	0.0112	4	12
MAX	0.46	0.0765	15	5

Table 2: Typical diffusion parameters that are compatible with the B/C analysis [30, 31]

The solution for the energy distribution, eq. 8, will generally be expressed as an integral equation

$$\psi(E, r_\odot) = \int_E^{m_\chi} dE_S \int d^3\mathbf{x}_S G(\mathbf{x}_\odot, E; \mathbf{x}_S, E_S) Q(\mathbf{x}_S, E_S) \tag{10}$$

where the last integral is performed over the diffusive halo. E_S is the energy at the source and $G(\mathbf{x}_\odot, E; \mathbf{x}_S, E_S)$ is the Green function which determines the probability for a cosmic ray produced at $\mathbf{x}_S$ with energy E_S to reach a detector at the Earth with an energy E. The differential flux is related to the number density

$$\Phi_a = \frac{v(E)}{4\pi} \psi_a \tag{11}$$

where v is the particle velocity. The method of solution of the general equation adapted to each type of charged cosmic rays will be described next.

3.2 Positrons

The energy spectrum of positrons is obtained by solving the diffusion-loss equation keeping only the two dominant contributions: space diffusion and energy losses.

$$-\nabla \cdot (K(E)\nabla\psi_{e^+}) - \frac{\partial}{\partial E}(b(E)\psi_{e^+}) = Q_{e^+}(\mathbf{x}, E) \tag{12}$$

Here $K = K_0(E/E_0)^\delta$ since for energies above 0.1 GeV the positrons are ultra relativistic and the rigidity $\mathcal{R}$ is proportionnal to E, $E_0 = 1 GeV$. The positron loss rate is dominated by synchrothon radiation in the galactic magnetic field and inverse Compton scattering on stellar light and CMB photons,

$$b(E) = \frac{E^2}{E_0 \tau_E} \tag{13}$$

where $\tau_E = 10^{16}$ s is the typical energy loss time. Subdominant contributions from diffusive reacceleration and galactic convection were shown to have an impact only below a few GeV's [38], these effects are not included in our treatment.

The propagation equation can be transformed into the heat conductivity equation after the substitutions

$$\psi(E, r, z) = \bar{N}(t, r, z)/b(E) \tag{14}$$

$$t(E) = -\int dE \frac{K(E)}{b(E)} \tag{15}$$

The propagation equation now reads

$$(\frac{\partial}{\partial t} - \nabla^2)\bar{N}(t,r,z) = \frac{\sigma v}{2m_\chi^2}\overline{\rho^2}(r,z)\left(\frac{f_{e^+}(E)b(E)}{K(E)}\right)\Bigg|_{E=E(t)} \tag{16}$$

Assuming $\overline{\rho^2}(r,z) = \overline{\rho^2(r,-z)}$, we can solve Eq. 16 in the region $0 < z < L$ with the boundary conditions

$$\bar{N}(t,r,L) = 0; \qquad \frac{\partial\bar{N}(t,r,z)}{\partial z}\Bigg|_{z=0} = 0 \tag{17}$$

The Green function for Eq. 16 can be factored into a r-dependent part, a Gauss function, and a z-dependent part. The latter is more complicated because of boundary conditions,

$$(\frac{\partial}{\partial \tau} - \nabla^2)\bar{G}(\tau,r,z,z') = \delta(\tau)\delta^2(\vec{r})\delta(z-z') \tag{18}$$

$$\bar{G}(\tau,r,z,z') = \frac{\Theta(\tau)}{4\pi\tau}exp(\frac{-r^2}{4\tau})g_v(\tau,z,z') \tag{19}$$

$$(\frac{\partial}{\partial \tau} - \frac{\partial^2}{\partial z^2})g_v(\tau,z,z') = \delta(\tau)\delta(z-z') \tag{20}$$

To calculate g_v, the vertical Green function, we construct a basis of eigenstates $e_n(z)$ of the operator $-\frac{d^2}{dz^2}$ defined on an interval $0 < z < L$ with the boundary conditions $e_n(L) = 0$ and $e'_n(0) = 0$. This basis is

$$e_n(z) = \sin(\pi(n+0.5)/L) \tag{21}$$

The vertical Green function expressed in terms of $e_n(z)$ reads

$$g_v(t,z,z') = \Theta(t)\sum_{n=0}^{\infty}e^{-k_n^2 t}e_n(z)e_n(z')/c_n \tag{22}$$

where c_n are the normalization constants

$$\int_0^L e_n(z)e_m(z)dz = \delta_{nm}c_n \tag{23}$$

When t is small, eq. 22 does not converge well. In this case g_v is rather obtained using the method of electrical images,

$$g_v(t,z,z') = \sum_{n=-\infty}^{\infty}\frac{(-1)^n}{\sqrt{4\pi\tau}}\left(e^{-\frac{(z-z'+2nL)^2}{4\tau}} + e^{-\frac{(z+z'+2nL)^2}{4\tau}}\right) \tag{24}$$

Using the Green functions, Eq. 18 - 20, the positron density near the Sun is obtained after

a $3D$ integration

$$\psi_{\bar{e}}(E_0, r_\odot, 0) = \frac{\sigma v}{b(E_0)} \int_{E_0}^{M_\chi} dE f(E) D(t(E_0) - t(E), r_\odot) \qquad (25)$$

$$D(0, r_\odot) = \frac{1}{2M_\chi^2} \overline{\rho^2(r_\odot, 0)} \qquad (26)$$

$$D(\tau, r_\odot) = \frac{1}{4\tau} \int_0^L dz g_v(\tau, z, 0) \int_0^\infty r dr \frac{\overline{\rho^2(r, z)}}{M_\chi^2} \exp\left(-\frac{(r - r_\odot)^2}{4\tau}\right) I_\phi\left(\frac{r_\odot r}{2\tau}\right) \quad (27)$$

$$I_\phi(x) = \frac{1}{\pi} \int_0^\pi d\phi e^{-2x \sin^2 \frac{\phi}{2}} = I_0(x) e^{-x} \qquad (28)$$

where I_0 is the modified Bessel function of the first kind. In practice we use R as the upper limit of the integral over r in Eq. 27. A more precise treatment of the boundary condition is not required as the positrons originating from far away sources suffer significant energy losses.

Note that $D(\tau, r_\odot)$ is an universal function for all energies. To calculate $\psi_{\bar{e}}(E)$ for all positron energies, it is more efficient to first tabulate D as a function of τ in the region $0 \le \tau \le t(E_{min}) - t(M_\chi)$ and then perform a fast integration for all energies. This is the method implemented in the `micrOMEGAs` routine `posiFluxTab`.

3.3 Antiprotons propagation

The propagation of antiprotons is dominated by diffusion and the effect of the galactic wind. The source term includes the annihilation of DM, Eq. 1, as well as a negative source term corresponding to the annihilation of antiprotons in the interstellar medium (H, He). The annihilation rate

$$\Gamma_{tot} = \sigma_{\bar{p}H}^{ann} v_{\bar{p}} n_H + \sigma_{\bar{p}He}^{ann} v_{\bar{p}} n_{He} \qquad (29)$$

where $v_{\bar{p}}$ is the velocity of the $\bar{p}$. The annihilation cross-sections $\sigma_{\bar{p}H}^{ann}$ are found in [34, 35] and rescaled by a factor $4^{2/3}$ for $\sigma_{\bar{p}He}^{ann}$. The average densities in the galactic disc are set to $n_H = 0.9$ and $n_{He} = 0.1$. The production of secondary antiprotons is not included in the code.

The energy spectrum of antiprotons is obtained by solving the diffusion equation

$$\left[-K(E)\nabla^2 + V_c \frac{\partial}{\partial z} + 2(V_c + h\Gamma_{tot}(E))\delta(z)\right] \psi_{\bar{p}}(E, r, z) = \frac{\sigma v}{2} \frac{\overline{\rho^2(r, z)}}{M_\chi^2} f_{\bar{p}}(E) \qquad (30)$$

An important difference with the positron case is that energy loss of antiprotons is negligible, we will therefore omit the E dependence until the final formula. $\partial \psi(r, z)/\partial z$ should have a discontinuity at $z = 0$. Assuming that $\rho^2(r, z) = \rho^2(r, -z)$ means that $\psi_{\bar{p}}(r, z)$ has the same symmetry and the discontinuity can be presented as a boundary condition

$$\left.\frac{\partial \psi_{\bar{p}}(r, z)}{\partial z}\right|_{z=0} = \psi_{\bar{p}}(r, 0)(V_c + h\Gamma_{tot})/K \qquad (31)$$

After substituting

$$\psi_{\bar{p}}(r, z) = \exp(k_c z) \bar{N}(r, z); \tag{32}$$

where $k_c = V_c/(2K)$, Eq. 30 simplifies to

$$\left[-\nabla^2 + k_c^2\right] \bar{N}(r, z) = e^{-k_c z} \frac{\sigma v}{2K} \frac{\overline{\rho^2(r, z)}}{M_\chi^2} f_{\bar{p}} \tag{33}$$

for $0 < z < L$ with the boundary conditions

$$\bar{N}(r, L) = 0; \qquad \frac{\partial \bar{N}(r, z)}{\partial z}\bigg|_{z=0} = \bar{N}(r, 0) v_d; \tag{34}$$

where $v_d = (V_c/2 + h\Gamma_{tot})/K$.

To compute the Green function for Eq. (33) we proceed as for the positron case and construct a basis of eigenstates of the $-\frac{d^2}{dz^2}$ operator defined on the interval $0 < z < L$ with the boundary conditions

$$e_n(z) = \sin\left(k_n(L - z)\right) \tag{35}$$

where the set of k_n is defined by the condition

$$e_n'(0) = e_n(0) v_d. \tag{36}$$

The Green function then reads

$$\bar{G}(r, z, z') = \frac{1}{2\pi} \sum_{n=0}^{\infty} K_0(r\sqrt{k_c^2 + k_n^2}) e_n(z) e_n(z')/c_n \tag{37}$$

where c_n are the normalization constants (see Eq. 23) and K_0 is a MacDonald function defined by the equation

$$\Delta_r K_0(r) - K_0(r) = -2\pi \delta^2(\vec{r}) \tag{38}$$

The antiproton energy spectrum at the Earth is obtained after a $3D$ integration

$$\psi_{\bar{p}}(E, r_\odot, 0) = \frac{\sigma v f_{\bar{p}}(E)}{K} \int_0^\infty r dr \int_0^L dz \bar{G}(r, z, 0) e^{-k_c z} \int_0^\pi d\phi \frac{\overline{\rho^2(r, z')}}{M_\chi^2} \tag{39}$$

with $r' = \sqrt{r_\odot^2 + r^2 + 2 r_\odot r \cos\phi}$.

To avoid numerical problems due to a possible singularity in the dark matter density near the center of the Galaxy, we integrate Eq. 39 in the central region $|x| < r_0 = 0.01 kpc$ fixing $\rho^2(|x|) = \rho^2(r_0)$, we then treat the $|x| < r_0$ region as a point-like source with $\rho^2(|x|) - \rho^2(r_0)$. The radial boundary conditions can be simulated by modifying the DM density. First we note that sources located at a distance $r > R$ have a negligible effect, we then take $\rho = 0$ when $r > R$. Second, radiation from a source located near the boundary $r \leq R$ will be suppressed. To estimate this suppression we add *mirror* sources with negative charges on each side of the boundary $r = R$. The long distance contribution from a point-like source is proportionnal to $K_0(r/a) \approx \exp(-r/a)$ where $a = 1/\sqrt{k_0^2 + k_c^2} \approx 2L/\pi$. We then modify the DM density

$$\rho^2(r, z) \quad \rightarrow \quad \Theta(R - r)\left(1 - \exp\left[-2(R - r)/a\right]\right) \rho^2(r, z) \tag{40}$$

13

The suppression factor is significant only in the region $R - L < r < R$.

The integrand in Eq. (39) ($I(E)$) is a smooth function that features only a slight energy dependence through the terms $K(E)$ and $\Gamma_{tot}(E)$. To provide a fast calculation of the antiproton spectrum we interpolate the function $I(E)$ in the range $M_\chi - E_{\min}$, and multiply this interpolated function by $f_{\bar{p}}(E)$ to obtain the final result for all E. $E_{\min}$ is defined by the user. Note that points for interpolation are added automatically until the required precision is reached.

3.3.1 Solar modulation

When charged particles propagate through the solar system, they are affected by the solar wind and lose energy. This effect leads to a shift in the energy distribution between the interstellar spectrum and the spectrum at the Earth, this shift affects the low energy part of the spectrum. We implement solar modulation using the force field approximation [36]. In this approximation the flux at the Earth is simply related to the flux at the heliospheric boundary (ϕ_h),

$$\frac{d\Phi_\odot}{dE_\odot} = \frac{p_\odot^2}{p_h^2} \frac{d\Phi_h}{dE_h} \tag{41}$$

where $p_\odot$ and p_h are the momenta at the Earth and the heliospheric boundary. The energies at the two locations are simply related by

$$E_\odot = E_{IS} - |Z| \phi_F \ , \tag{42}$$

where the Fisk potential ϕ_F varies between 300MV to 1000MV from the minimum to the maximum of solar activity. The default value is set to 500MV.

4 Functions of micromegas

A complete description of all `micrOMEGAs` functions is available in the online manual, `http://lappweb.in2p3.fr/lapth/micromegas/`. This updated manual is also provided with the code, the file `manual4.tex` can be found in the main `micrOMEGAs` 2.4 directory. Here we describe the functions that are specific to the indirect detection module. A new feature of version 2.4 is the use of global parameters. A list of the global parameters relevant for the indirect detection module and their default values are given in Table 1. The numerical value for any of these parameters can be simply reset anywhere in the code.

4.1 Spectra interpolation and display

Various spectra of SM particles produced in DM annihilation processes are stored in arrays containing NZ=250 elements. The ith element of an array corresponds to dN/dz_i where $z_i = \log(E_i/M_\chi)$. Here `E_i` is the kinetic energy of the particle and N stands for either the number of particles or a particle flux in $(\text{cm}^2 \text{s sr})^{-1}$.[3]

The following functions can be used for interpolation and visualization

---

[3] Although not needed if one uses the interpolation functions, the value of z_i can be obtained by the function $Zi(i)$. In the current version $Zi(i) = log(10^{-7})(i/NZ)^{1.5}$.

Name	Default value	Units	Comments
Mcdm		GeV	Mass of Dark Matter particle, M_χ
Rsun	8.	kpc	Distance from the Sun to the Galactic center, $r_\odot$
rhoDM	0.3	GeV/cm^3	Dark Matter density at Rsun, $\rho_\odot$
Rdisk	20	kpc	Radius of the galactic diffusion disk, R
K_dif	0.0112	kpc^2/Myr	Diffusion coefficient K_0
L_dif	4	kpc	Half height of the galactic diffusion zone L
Delta_dif	0.7		Slope of diffusion coefficient, δ
Tau_dif	10^{16}	s	Positron energy loss time scale, τ_E
Vc_dif	12	km/s	Convective velocity of Galactic vind , V_C

Table 3: Global parameters of the indirect detection module

- `SpectdNdE(E,spectTab)`
interpolates the tabulated spectra and returns the `dN/dE` distribution where `E` is the energy in GeV.
- `zInterp(z,SpectTab)`
interpolates the tabulated spectra and returns the `dN/dz` distribution where $z = \log(E/M_\chi)$, here $z = 0$ corresponds to $E = M_\chi$.
- `displaySpectrum(Spectrum,message,Emin,Emax,Units)`
displays the resulting spectrum, `message` is a text string which gives a title to the graphic plot. `Emin` and `Emax` define energy cuts. If `Units=0` the spectrum is written as a function of z otherwise the spectrum is a function of the energy in GeV.

4.2 Annihilation spectra

- `calcSpectrum(key,Sg,Se,Sp,Sne,Snm,Snl,&err)`
calculates the spectra of DM annihilation at rest and returns σv in cm^3/s . The calculated spectra for γ, e^+, $\bar{p}$, ν_e, ν_μ, ν_τ are stored in arrays of dimension NZ as described above: `Sg`, `Se`, `Sp`, `Sg`, `Sne`, `Snm`, `Snl`. To remove the calculation of a given spectra, substitute `NULL` for the corresponding argument. `key` is a switch to include polarisation of W,Z bosons (`key=1`) or photon radiation (`key=2`). Photon radiation is added to all subprocesses when computing the photon spectrum while only the 3-body process $\chi\chi \to e^+e^-\gamma$ is included for the positron spectrum. When `key=4` the cross sections for each annihilation channel are written on the screen. More than one option can be switched on simultaneously by adding the corresponding values for `key`. For example both the W polarisation and photon radiation effects are included if `key=3`. A problem in the spectrum calculation will produce a non zero error code, $err \neq 0$.
- `spectrInfo(Xmin,spectrTab,&Ntot,&Xtot)`
provides information on the spectra generated. Here `Xmin` defines the minimum cut for the energy fraction x=E/Mcdm, `Ntot` and `Xtot` are calculated parameters which give on average the total number and the energy fraction of the final particles produced per collision. Note that the upper limit is Xtot=2.
- `basicSpectra(pdgN,outN,Spectr)`
is a routine for model independent studies that computes the spectra of outgoing particles as obtained by PYTHIA and writes the result in an array of dimension 250, `Spectr`. `pdgN`

is the PDG code of the particles produced in the annihilation of a pair of dark matter particles. The spectrum for polarised W's or Z's is obtained by substituting `pdgN+'T'` (transverse) or `pdgN+'L'` (longitudinal) for the PDG code of the W(Z), `pdgN=24(23)`. `outN` specifies the outgoing particle,

$$\text{outN} = \{0, 1, 2, 3, 4, 5\} \text{ for } \{\gamma, e^+, p^-, \nu_e, \nu_\mu, \nu_\tau\}$$

Note that the propagation routines for $e^+, \bar{p}, \gamma$ can be used after this routine as usual.
- `loopGamma(&vcs_gz,&vcs_gg)`
calculates σv in cm^3/s for the loop induced neutralino annihilation into γZ and $\gamma\gamma$. In case of problem the function returns a non-zero value. This function is available only for the MSSM.

4.3   Distribution of Dark Matter in the Galaxy.

To compute the signal from an indirect detection experiment one has to take into account the dark matter distribution in the Galaxy. Both the DM density profile as well as the clump profile, Eq. 3, have to be defined. The DM density at the Sun, $\rho_\odot$ as well as $r_\odot$, the distance from the center of the Galaxy to the Sun are defined by the global variables `rhoDM` and `Rsun`.
- `setHaloProfiles(`F_{halo}, F_{clump}`)`
allows to change both the halo and the clump profile. Any sphericaly symmetric DM halo profile can be defined.
- `hProfileABG(r)`
is the default halo density profile, Eq. 3
- `setProfileABG(alpha,beta,gamma,a)`
resets the parameters of the DM distribution profile. The default parameters correspond to the NFW profile, $\alpha = 1, \beta = 3, \gamma = 1, a = 20[kpc]$.
- `hProfileEinasto(r)`
is the Einasto halo density profile, eq. 4.
- `setProfileEinasto(alpha)`
sets the parameter α for the Einasto profile, the default value is $\alpha = 0.17$.
- `noClumps(r)`
is a non clumpy profile which is used by default. It returns 1 for any argument.

4.4   Particle propagation.

The spectrum of charged particles observed strongly depends on their propagation in the Galactic Halo. The propagation depends on the global parameters

        `K_dif, Delta_dif, L_dif, Rsun, Rdisk`

as well as

 `Tau_dif (positrons), Vc_dif (antiprotons)`

- `posiFluxTab(Emin,sigmav, Se,  Sobs)`
computes the positron flux at the Earth. Here `sigmav` and `Se` are values obtained by `calcSpectrum`. `Sobs` is the positron spectrum after propagation. `Emin` is the energy cut

to be defined by the user. Note that a low value for `Emin` increases the computation time. The format is the same as for the initial spectrum. The function `SpectrdNdE(E,Sobs)` described above can also be used for interpolation, in this case the flux returned in (GeV s cm^{2}sr)$^{-1}$).

• `pbarFlux(E,dSigmavdE)`

computes the antiproton flux for a given energy `E` and a differential cross section for antiproton production, `dSigmavdE`. For example, one can substitute

`dSigmavdE`=σv`SpectdNdE(E,SpP)`

where σv and SpP are obtained by `calcSpectrum`. This function does not depend on the details of the model and allows to analyse the dependence on the parameters of the propagation model.

• `pbarFluxTab(Emin,sigmav, Sp,  Sobs)`

computes the antiproton flux, this function works like `posiFluxTab`,

• `solarModulation(Phi, mass, stellarTab, earthTab)`

takes into account modification of the interstellar positron/antiproton flux caused by the electro-magnetic fields in the solar system. Here `Phi` is the effective Fisk potential in MeV, `mass` is the particle mass, `stellarTab` describes the interstellar flux, `earthTab` is the calculated particle flux in the Earth orbit.

The photon flux does not depend on the diffusion model parameters but on the angle ϕ between the line of sight and the center of the galaxy as well as on the annihilation spectrum into photons

• `gammaFluxTab(fi,dfi,sigmav,Sg,Sobs)`

multiplies the annihilation photon spectrum with the integral over the line of sight and over the opening angle to give the photon flux. `fi` is the angle between the line of sight and the center of the galaxy, `dfi` is half the cone angle which characterizes the detector resolution (the solid angle is $2\pi(1 - cos(dfi))$, `sigmav` is the annihilation cross section, `Sg` is the DM annihilation spectra. `Sobs` is the spectra observed. Note that `Emin` is not specified, since this function is not time consuming the integration is done for all energies.

The function `gammaFluxTab` can be used for the neutrino spectra as well.

• `gammaFlux(fi,dfi,vcs)`

is the same function as `gammaFluxTab` above but corresponds to a discrete photon spectrum. `vcs` is the annihilation cross section, for instance in the $\hat{\text{M}}$SSM it is calculated with the `loopGamma` function. The function returns the number of photons per cm^2 of detector surface per second. Note that for $\chi\chi \to \gamma\gamma$ the result should be multiplied by a factor 2 as each annihilation leads to the production of two photons.

Note that for `solarModulation` and for all `*FluxTab` routines one can use the same array for the spectrum before and after propagation.

5   Examples and results

5.1   Sample output

Running the main.c sample file in the `micrOMEGAs`/MSSM directory choosing the options `MASSES_INFO,CONSTRAINTS,OMEGA`, `INDIRECT_DETECTION`, `CDM_NUCLEON` will lead to the following output.

```
========= SLHA file input =========
Initial file  "model2.slha"
Warnings from spectrum calculator:
Model: model2

Dark matter candidate is '~o1' with spin=1/2  mass=1.48E+02

~o1 = 0.833*bino -0.114*wino -0.448*higgsino1 -0.303*higgsino2

=== MASSES OF HIGGS AND SUSY PARTICLES: ===
Higgs masses and widths
     h   123.08 2.59E-03
     H  1000.20 1.19E+01
    H3  1000.00 1.20E+01
    H+   998.63 1.18E+01


Masses of odd sector Particles:
~o1  : MNE1  =    147.7 || ~2+  : MC2   =   189.9 || ~o2  : MNE2  =   198.2
~o3  : MNE3  =    211.1 || ~o4  : MNE4  =   345.1 || ~1+  : MC1   =   345.3
~g   : MSG   =   1108.9 || ~t1  : MSt1  =  2418.8 || ~b1  : MSb1  =  2496.4
~ne  : MSne  =   2499.2 || ~nm  : MSnm  =  2499.2 || ~nl  : MSnl  =  2499.2
~uL  : MSuL  =   2499.4 || ~cL  : MScL  =  2499.4 || ~uR  : MSuR  =  2499.8
~cR  : MScR  =   2499.8 || ~l1  : MSl1  =  2499.8 || ~sL  : MSsL  =  2500.1
~dL  : MSdL  =   2500.1 || ~mL  : MSmL  =  2500.3 || ~eL  : MSeL  =  2500.4
~eR  : MSeR  =   2500.4 || ~mR  : MSmR  =  2500.5 || ~dR  : MSdR  =  2500.7
~sR  : MSsR  =   2500.7 || ~l2  : MSl2  =  2501.0 || ~b2  : MSb2  =  2504.4
~t2  : MSt2  =   2589.4 ||



==== Physical Constraints: =====
deltartho=5.70E-06
gmuon=-8.31E-11
bsgnlo=3.94E-04
bsmumu=3.02E-09
btaunu=9.96E-01
MassLimits OK

==== Calculation of relic density =====
Xf=2.45e+01 Omega=1.13e-01


Channels which contribute to 1/(omega) more than 1%.
Relative contrubutions in % are displyed
 60% ~o1 ~o1 -> W+ W-
 26% ~o1 ~o1 -> Z Z
  9% ~o1 ~o1 -> Z h
  1% ~o1 ~o1 -> h h
The rest 3.28 %


==== Indirect detection =======
    Channel           vcs[cs^3/s]
```

```
  ~o1,~o1 -> h h        1.30E-43
  ~o1,~o1 -> Z h        1.31E-27
  ~o1,~o1 -> Z Z        5.03E-27
  ~o1,~o1 -> W+ W-      1.20E-26
sigmav=1.83E-26[cm^3/s]
Photon flux  for angle of sight f=0.00[rad]
and spherical region described by cone with angle 0.04[rad]
Photon flux = 2.01E-14[cm^2 s GeV]^{-1} for E=73.8[GeV]
Gamma  ray lines:
E=1.34E+02[GeV]  vcs(Z,A)= 1.37E-29[cm^3/s], flux=7.19E-14[cm^2 s]^{-1}
E=1.48E+02[GeV]  vcs(A,A)= 2.47E-30[cm^3/s], flux=2.58E-14[cm^2 s]^{-1}
N_=19
Positron flux  =  8.09E-12[cm^2 sr s GeV]^{-1} for E=73.8[GeV]
N_grid=9
Antiproton flux  =  1.77E-11[cm^2 sr s GeV]^{-1} for E=73.8[GeV]

==== Calculation of CDM-nucleons amplitudes  =====
CDM-nucleon micrOMEGAs amplitudes:
proton: SI -4.570E-09  SD  -6.116E-07
neutron: SI -4.582E-09  SD  5.355E-07
CDM-nucleon cross sections[pb]:
 proton  SI 9.015E-09  SD 4.844E-04
 neutron SI 9.061E-09  SD 3.714E-04
```

5.2 Comparison with other packages

We have performed many tests to check the consistency of the results obtained with `micrOMEGAs`. For the treatment of the hadronization process, we have computed the fragmentation functions with `PYTHIA`(those are implemented in `micrOMEGAs`) and with `HERWIG`. Despite the fact that the two codes are based on different modelling of the hadronization process, the functions dN/dE obtained with `PYTHIA` and `HERWIG` are very similar. A comparison between the two codes in the case of a 500 GeV annihilating into $b\bar{b}$ pairs has been performed and gave similar results.

	Model 1		Model 2	
	$\mu = -440, M_A = 1000$		$\mu = -200, M_A = 1000$	
	$M_2 = 800, M_0 = 2500$		$M_2 = 320, M_0 = 2500$	
	$A_t = A_b = 1000$		$A_t = -A_b = -2500$	
	$\tan\beta = 10$		$\tan\beta = 8.$	
	microMEGAs	DarkSusy	microMEGAs	DarkSusy
M_χ (GeV)	386.7	386.7	147.7	147.7
$\sigma v(\mathrm{cm}^3\mathrm{s}^{-1})$	1.97×10^{-26}	2.32×10^{-26}	1.83×10^{-26}	1.97×10^{-26}
Main final states	$t\bar{t}$ (77.7%)	$t\bar{t}$ (80.4%)	W^+W^- (65.6%)	W^+W^- (65.2%)
	W^+W^- (8.9%)	W^+W^- (8.1%)	Z^0Z^0 (27.5%)	Z^0Z^0 (26.8%)
	ZZ (6.5%)	ZZ (5.8%)	Z^0h (7.2%)	Z^0h (7.2%)

Table 4: Main features of the two sets of parameters used for the comparison

For the signal itself, we compare the results obtained with `DarkSusy` 5.0.4 and `micrOMEGAs`2.4.

To perform the comparison, we generate MSSM points with `DarkSusy` and used the resulting SLHA file [39] as an input for `micrOMEGAs`. Each package computes the annihilation cross-section, branching ratios, propagation and distribution. We have chosen two sample models in the MSSM, the input parameters at the weak scale are specified in Tab. 4 where all dimensionful parameters are in GeV. We assume $2M_1 = M_2 = M_3/3$ as would be obtained in a GUT model with gaugino mass universality, a common sfermion mass at the weak scale, m_0 and vanishing trilinear couplings of sleptons and of the first and second generations of squarks. The files used for this comparison are provided in the MSSM directory of `micrOMEGAs`(`model1.slha` and `model2.slha`). The main features of the sample models are summarized in Tab. 4. The first obsevation is that the total annihilation cross section as well as the individual channel contribution can vary by up to 17%. This is particularly important if the main annihilation channels are into third generation quarks (Model 1). Indeed `DarkSusy` and `micrOMEGAs` use a different prescription for the running of quark Yukawa couplings. Part of the difference between the two codes is due to a different prescription for $\sin^2 \theta_W$, an On-Shell scheme in `DarkSusy` and $\overline{MS}$ in `micrOMEGAs`.

To compare the γ-ray spectrum, we use an NFW profile and compute the signal from the Galactic center in a cone of 1° opening angle (corresponding to a solid angle of $\Delta\Omega = 10^{-3}$ sr). Fig. 3 displays the results for both models. For this we have switched on the gauge boson polarisation and included the contribution from 3-body final states with a photon. The small difference between the two spectra is explained by the difference in σv. Notice that on these plots, the flux is E^2-corrected.

For the one-loop processes leading to a monochromatic gamma-ray line, a detailed comparison between `DarkSusy` and SloopS was performed in [21]. The two codes agreed very well for the annihilation of a neutralino pair into two photons. We also find good agreement ($< 5\%$) between `micrOMEGAs` and `DarkSusy` for our two test models. On the other hand in [21] it was pointed out that large differences between `DarkSusy` and `SloopS` can occur for the γZ one-loop process ($> 30\%$). This is mainly because some diagrams were neglected in `DarkSusy`, these give a non negligible contribution for the case of a higgsino LSP.
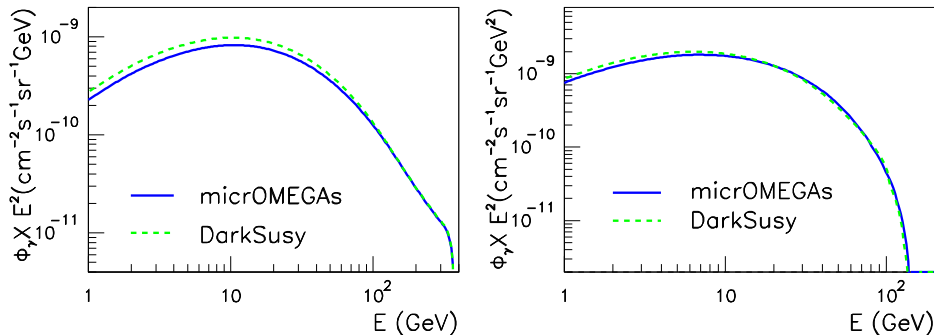

Figure 3: γ-ray signal for Model 1(left) and Model 2(right) with `micrOMEGAs` and `DarkSusy`

In the case of positrons, the comparison is shown on Fig. 4. The propagation pa-

rameters are the default parameters of `DarkSusy` , $R = 30\text{kpc}$, $h = 0.1\text{kpc}$, $L = 4\text{kpc}$, $K_0 = 0.0826\text{kpc}^2/\text{Myr}$, $\delta = 0.6$, $V_C = 10\text{km/s}$. Note that the space diffusion coefficient K is defined at a reference energy of 4GeV in `DarkSusy` rather than 1GeV in `micrOMEGAs` . To reproduce similar propagation parameters one must therefore rescale the coefficient K_0 in `micrOMEGAs`. Furthermore for positrons `DarkSusy` assumes that $\delta = 0$ below $p = 4\text{GeV}$. The difference between the two codes is small (few percent) once taking into account the correction due to the initial σv. Larger differences are found at low energies and could be due to the different treatment of the positron propagation in that energy range. However, as shown below in section 5.3, the observed differences are much below the theoretical uncertainty induced by the propagation parameters. Good agreement between the two codes is also recovered for the antiproton signal, see Fig. 5.
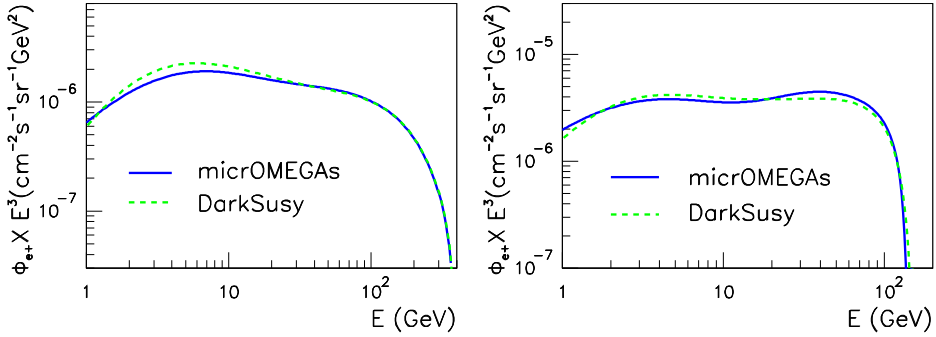

Figure 4: Positron signal for Model 1(left) and Model 2(right) with `micrOMEGAs` and `DarkSusy`. Here we have set $\delta = 0.6$, $K_0 = 0.03607$ kpc^2/Myr, $L = 4$ kpc and $V_C = 10$ km/s.
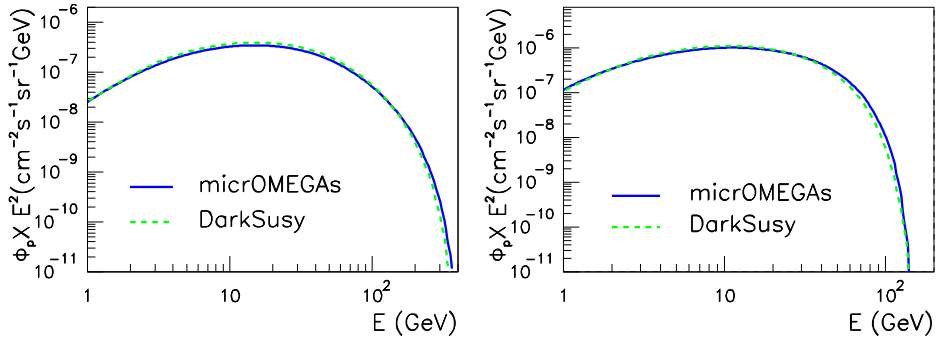

Figure 5: Antiproton signal for Model 1(left) and Model 2(right) with `micrOMEGAs` and `DarkSusy`. Same propagation parameters as above. Solar modulation is included with $\phi_F = 320$ MV.

5.3 Theoretical uncertainties related to propagation

The way the propagation of charged particles is handled in the code allows to very quickly estimate the propagation related uncertainty. For this we compare antiprotons and positrons signals using extreme values for the propagation parameters that are still allowed by all cosmic ray measurements. The curves labelled "Min", "Med", "Max" in Fig. 6 correspond to the parameters specified in Tab. 2. Recall that these parameters were selected to reproduce the data on the B/C ratio [30, 31]. For antiprotons the uncertainty exceeds one order of magnitude over the full range of energy while for positrons the uncertainty is large mainly at low energies. Actually high energy positrons do not suffer from propagation uncertainties since they are produced locally.
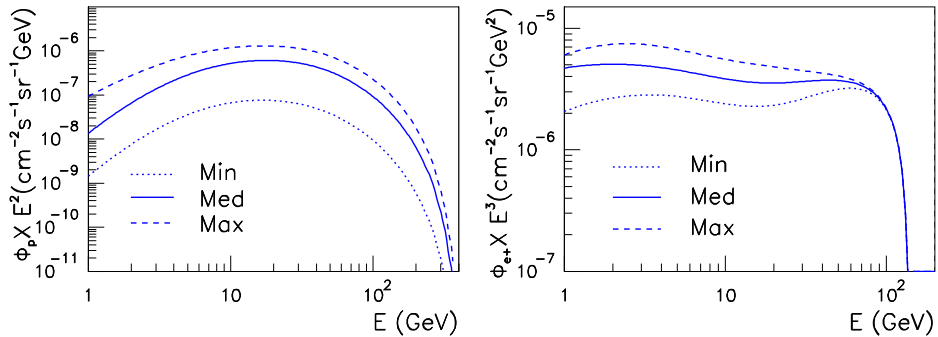

Figure 6: Propagation related uncertainty for antiprotons in Model 1(left) and for positrons in Model 2 (right). The propagation parameters are listed in Table 2.

6 Conclusions

With the new module for indirect detection presented here, `micrOMEGAs` is a comprehensive code for the study of the properties of weakly interacting cold dark matter candidates in various extensions of the standard model. The main features of this new version include the propagation of charged cosmic rays and some higher order processes in DM annihilation. In particular the code contains a full computation of photon radiation. These new features are available for any model with a weakly interacting particle that is already implemented in `micrOMEGAs`. In addition a specific code for the computation of the loop-induced gamma-ray line in the MSSM is included. The modular and flexible structure of the code makes it simple for the user to improve some specific part of the code, for example adding new functions that take into account the presence of dark matter clumps. The main observable that is not yet included in the code is the neutrino signal associated with dark matter capture in the Sun or in the Earth. This feature will be available in the next upgrade of `micrOMEGAs`. The code is available at http://lappweb.in2p3.fr/lapth/micromegas/.

Acknowledgements

References

[1] O. Adriani *et al.* [PAMELA Collaboration], Nature **458** (2009) 607 [arXiv:0810.4995 [astro-ph]].

[2] J. J. Beatty *et al.*, Phys. Rev. Lett. **93** (2004) 241102 [arXiv:astro-ph/0412230].

[3] M. Aguilar *et al.* [AMS-01 Collaboration], Phys. Lett. B **646** (2007) 145 [arXiv:astro-ph/0703154].

[4] O. Adriani *et al.*, Phys. Rev. Lett. **102** (2009) 051101 [arXiv:0810.4994 [astro-ph]].

[5] A. A. Abdo *et al.* [The Fermi LAT Collaboration], arXiv:0905.0025 [astro-ph.HE].

[6] J. Chang *et al.*, Nature **456** (2008) 362.

[7] F. Aharonian *et al.* [H.E.S.S. Collaboration], arXiv:0905.0105 [astro-ph.HE].

[8] A. W. Strong *et al.*, Astron. Astrophys. **444** (2005) 495 [arXiv:astro-ph/0509290].

[9] G. Maier and f. t. V. collaboration, AIP Conf. Proc. **1085** (2009) 187 [arXiv:0810.0515 [astro-ph]].

[10] D. J. Thompson, Rept. Prog. Phys. **71** (2008) 116901 [arXiv:0811.0738 [astro-ph]].

[11] F. Aharonian *et al.* [H.E.S.S. Collaboration], Nature **439** (2006) 695 [arXiv:astro-ph/0603021].

[12] F. Aharonian [HESS collaboration], arXiv:0904.0361 [astro-ph.HE].

[13] C. Meurer and FermiLAT collaboration, AIP Conf. Proc. **719** (2009) 1085 [arXiv:0904.2348 [astro-ph.HE]].

[14] G. Bélanger, F. Boudjema, A. Pukhov and A. Semenov, Comput. Phys. Commun. **174** (2006) 577 [arXiv:hep-ph/0405253].

[15] G. Bélanger, F. Boudjema, A. Pukhov and A. Semenov, Comput. Phys. Commun. **180** (2009) 747 [arXiv:0803.2360 [hep-ph]].

[16] G. Bélanger, F. Boudjema, A. Pukhov and A. Semenov, Comput. Phys. Commun. **176** (2007) 367 [arXiv:hep-ph/0607059].

[17] P. Gondolo, J. Edsjo, P. Ullio, L. Bergstrom, M. Schelke, E.A. Baltz, 2004, JCAP, 0407, 008.

[18] A. Pukhov, arXiv:hep-ph/0412191.

[19] T. Sjöstrand, *et al.*, Comput. Phys. Commun. **135** (2001) 238.

[20] L. Bergstrom, Phys. Lett. B **225** (1989) 372.

[21] F. Boudjema, A. Semenov and D. Temes, Phys. Rev. D **72** (2005) 055024 [arXiv:hep-ph/0507127].

[22] N. Baro, F. Boudjema and A. Semenov, Phys. Rev. D **78** (2008) 115003 [arXiv:0807.4668 [hep-ph]].

[23] E. Boos *et al.*, arXiv:hep-ph/0109068.

[24] T. Bringmann, L. Bergstrom and J. Edsjo, JHEP **0801** (2008) 049 [arXiv:0710.3169 [hep-ph]].

[25] J. Einasto, Trudy Inst. Astroz. Alma-Ata**51** (1965) 87.

[26] J. Lavalle, Q. Yuan, D. Maurin and X. J. Bi, arXiv:0709.3634 [astro-ph].

[27] D. Hooper, J. E. Taylor and J. Silk, Phys. Rev. D **69** (2004) 103509 [arXiv:hep-ph/0312076].

[28] V. S. Berezinskii, S. V. Buolanov, V. A. Dogiel, V. L. Ginzburg and V. S. Ptuskin, Astrophysics of Cosmic Rays, Amsterdam: North-Holland (1990).

[29] V. S. Ptuskin, H. J. Voelk, V. N. Zirakashvili, D. Breitschwerdt, A & A **321** (1997) 434.

[30] D. Maurin, F. Donato, R. Taillet and P. Salati, Astrophys. J. **555**, 585 (2001) [arXiv:astro-ph/0101231].

[31] F. Donato, N. Fornengo, D. Maurin, P. Salati, Phys. Rev. **D69** (2004) 063501 [arXiv:astro-ph/0306207].

[32] F. Donato, D. Maurin, P. Salati, A. Barrau, G. Boudoul and R. Taillet, Astrophys. J. **563** (2001) 172 [arXiv:astro-ph/0103150].

[33] F. Donato, N. Fornengo and D. Maurin, Phys. Rev. D **78** (2008) 043506 [arXiv:0803.2640 [hep-ph]].

[34] L. C. Tan and L. K. Ng, Phys. Rev. D **26**, 1179 (1982).

[35] L. C. Tan and L. K. Ng, J. Phys. G **9** (1983) 1289.

[36] J. S. Perko, Astronomy & Astrophysics **184** (1987) 119.

[37] R. Mohayaee and P. Salati, 2008 [arXiv:0801.3271[astro-ph]].

[38] T. Delahaye *et al.,* Astron. Astrophys. **501** (2009) 821 [arXiv:0809.5268[astro-ph]].

[39] B. Allanach *et al.*, Comput. Phys. Commun. **180** (2009) 8 [arXiv:0801.0045 [hep-ph]].

[40] J. Alcaraz, *et al*, 2002, Nucl. Instrum. Meth. A, 478, 119